

See discussions, stats, and author profiles for this publication at: <https://www.researchgate.net/publication/231652209>

# Chemisorption of Transition-Metal Atoms on Boron- and Nitrogen-Doped Carbon Nanotubes: Energetics and Geometric and Electronic Structures

ARTICLE *in* THE JOURNAL OF PHYSICAL CHEMISTRY C · APRIL 2009

Impact Factor: 4.77 · DOI: 10.1021/jp9000913

---

CITATIONS

49

READS

23

## 2 AUTHORS, INCLUDING:



Wei An

Shanghai University of Engineering Science

47 PUBLICATIONS 1,094 CITATIONS

SEE PROFILE

Article

## Chemisorption of Transition-Metal Atoms on Boron- and Nitrogen-Doped Carbon Nanotubes: Energetics and Geometric and Electronic Structures

Wei An, and C. Heath Turner

*J. Phys. Chem. C*, **2009**, 113 (17), 7069-7078 • DOI: 10.1021/jp9000913 • Publication Date (Web): 03 April 2009

Downloaded from <http://pubs.acs.org> on April 24, 2009

### More About This Article

Additional resources and features associated with this article are available within the HTML version:

- Supporting Information
- Access to high resolution figures
- Links to articles and content related to this article
- Copyright permission to reproduce figures and/or text from this article

[View the Full Text HTML](#)



ACS Publications

High quality. High impact.

The Journal of Physical Chemistry C is published by the American Chemical Society. 1155 Sixteenth Street N.W., Washington, DC 20036

# Chemisorption of Transition-Metal Atoms on Boron- and Nitrogen-Doped Carbon Nanotubes: Energetics and Geometric and Electronic Structures

Wei An and C. Heath Turner\*

Department of Chemical and Biological Engineering, The University of Alabama,  
Tuscaloosa, Alabama 35487-0203

Received: January 5, 2009; Revised Manuscript Received: February 19, 2009

The well-defined binding between transition-metals (TM) and the sidewall of carbon nanotubes (CNTs) plays a key role in the performance of CNT-based nanoelectronics, as well as the stability of catalysts used in either heterogeneous catalysis or fuel-cell electrocatalysis. Spin-polarized density functional theory calculations demonstrate that either boron or nitrogen doping can increase the binding strength of TM atoms with single-wall carbon nanotubes (SWCNTs), and comparatively, boron doping is more effective. The binding nature can be identified as chemisorption, based on the magnitude of the binding energy and the formation of multiple bonds. The chemisorbed TM atoms can modify the electronic structure of the doped nanotubes in various ways, depending upon the TM and helicity of the CNT, rendering the TM/doped-SWCNT composite viable for a wide range of applications. A total of 11 technologically relevant TMs adsorbed on two distinct and stable doped-SWCNT models have been investigated in this study. The doping sites are arranged in either a locally concentrated or uniform fashion within semiconducting SWCNT(8,0) and metallic SWCNT(6,6). The results serve as a starting point for studying larger, more complex TM nanostructures anchored on the sidewall of boron- or nitrogen-doped CNTs.

## 1. Introduction

The unique electronic, geometric, and mechanical properties of carbon nanotubes (CNTs) have stimulated wide scientific interest since their experimental realization and characterization in the laboratory over a decade ago.<sup>1–5</sup> They have been extensively studied in various applications, such as building blocks in nanoelectronics, optoelectronics,<sup>6</sup> and spintronic devices,<sup>7</sup> and as a support for heterogeneous catalysis<sup>8</sup> and fuel-cell electrocatalysis,<sup>9</sup> gas sensors,<sup>10</sup> and more.<sup>11–13</sup> In parallel, enhancing the functionality of CNTs with transition-metal nanoparticles (TMNPs) has also been intensively studied.<sup>14</sup> Hybrid TMNP/CNT composites have found many applications similar to CNTs, especially in the field of catalysis. Interestingly, CNTs may also act as templates for TMNP growth, which may alter the size and shape of the TMNPs.

When TM/CNT materials serve as the key components in field-effect transistors (FETs) and nanoelectrodes,<sup>15–21</sup> or are used as a catalyst, a central issue is the binding nature between the TM and the sidewall of the CNTs. As expected, for reliable performance in nanoelectronics or catalysis, the intimate contact (binding) between the CNTs and the TMs is crucial. However, the binding nature at the interface between the TMs and the pristine CNTs is poorly defined, and in most cases, can be classified as a van der Waals-type interaction.<sup>22</sup>

CNTs are known to be intrinsically either semiconducting or metallic,<sup>11</sup> which sensitively depends upon the chirality and diameter of the nanotubes,<sup>1–4</sup> and mixtures of such CNTs are generally produced in the synthesis process. Considering the challenging fabrication of large supplies of CNTs with specific chirality and radius, chemical doping, e.g., boron and nitrogen doping, of CNTs may serve as an alternative route for controlling the electronic characteristics of CNTs for specific

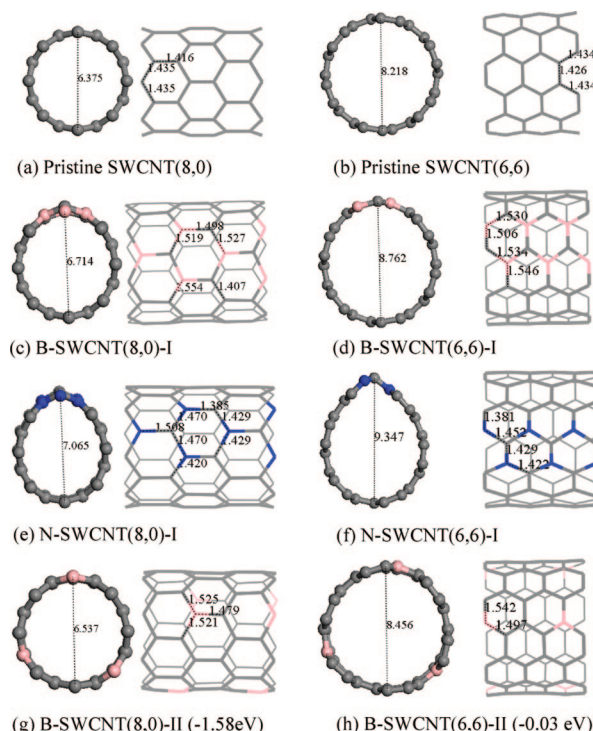


**Figure 1.** Optimized structures (top and side view) of pristine single-wall carbon nanotubes (SWCNTs), boron-doped carbon nanotubes (B-SWCNTs), and nitrogen-doped carbon nanotubes (N-SWCNTs). Nanotubes of one supercell size are shown in the figure. Diameter and typical bond lengths ( $\text{\AA}$ ) near the doping sites are labeled. Isomer structures (type II) of (c) and (d) are shown in (g) and (h), respectively, but with lower total energy per supercell (in parentheses). The shorter diameters for (c), (d), (e), and (f) are 6.222, 8.062, 5.740, and 7.346  $\text{\AA}$ , respectively.

\* To whom correspondence should be addressed. E-mail: hturner@eng.ua.edu.

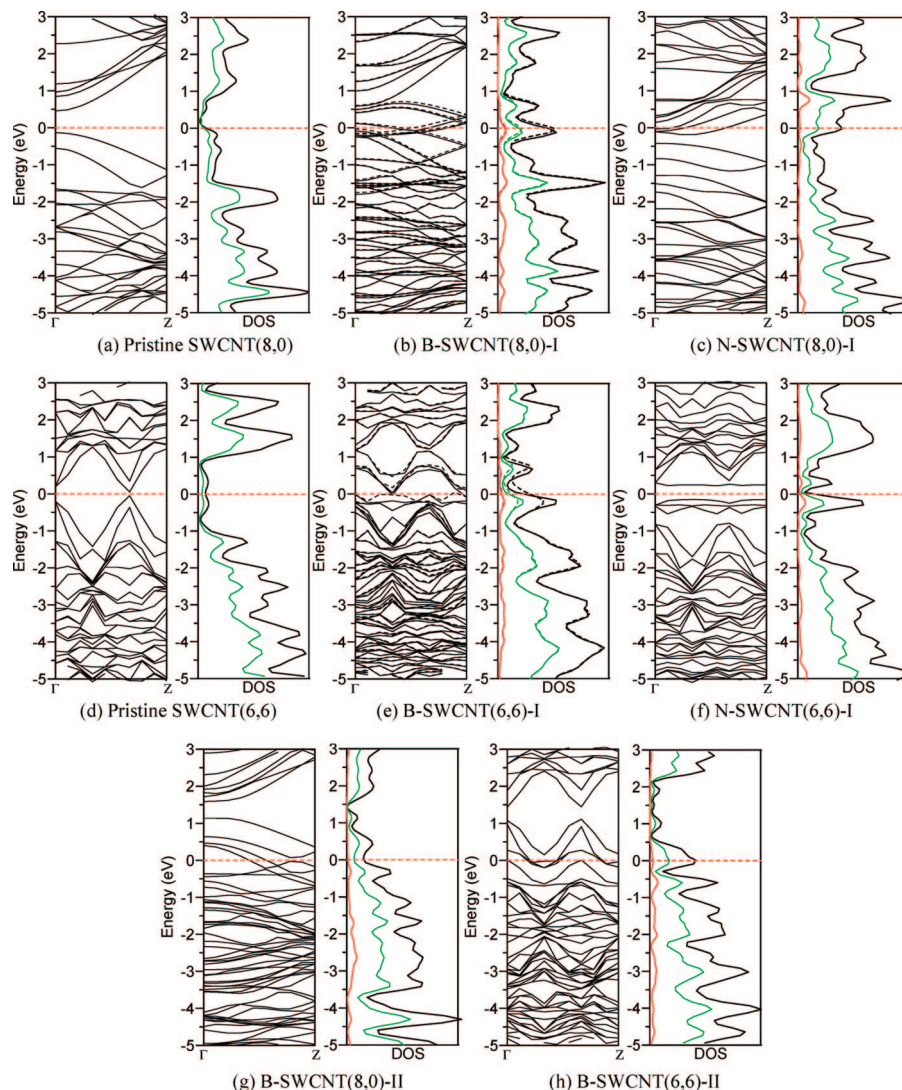


**Figure 2.** Calculated band structure and density of states (DOS) for pristine SWCNTs and doped-SWCNTs. Green and red represent projected C-*p* and B-*p* (or N-*p*) state, respectively. Fermi level (red dash line) is shifted to zero eV. The spin-down state is shown by the dashed line.

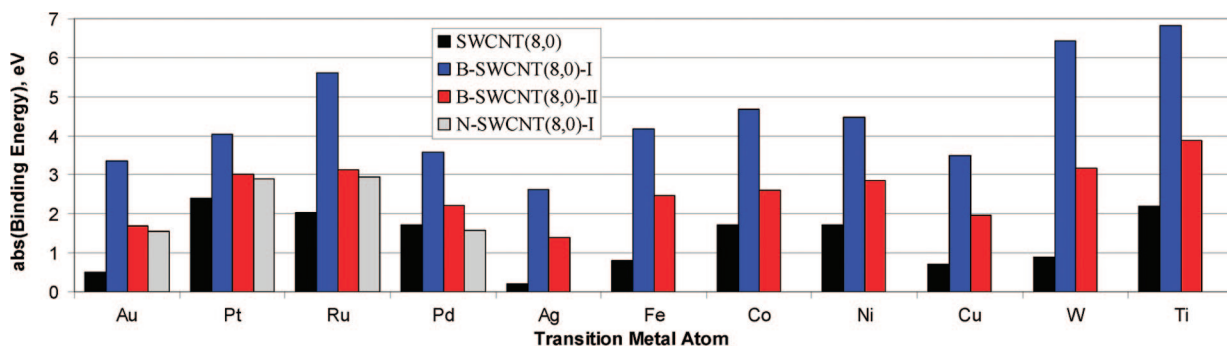


**Figure 3.** Calculated binding energy of the TM atoms on the various SWCNT(8,0) models. The results on the pristine SWCNT(8,0) are taken from ref 22, except for the Ru atom (which we have calculated).

needs. Furthermore, the feasibility of tailoring the structural and electronic properties of CNTs by using boron and nitrogen doping have already been realized in many experiments.<sup>23–29</sup> Our previous study<sup>30</sup> of boron- and nitrogen-doped graphene has shown that boron doping can significantly enhance the binding strength of the graphene with TMs, such as Pt and Ru clusters. A similar trend may also be realized on CNTs. However, to our knowledge, no theoretical studies have reported

the behavior of transition metals adsorbed on boron- and nitrogen-doped SWCNTs.

In this work, we report density-functional theory (DFT) calculation results of eleven TM atoms (i.e., Au, Pt, Ru, Pd, Ag, Fe, Co, Ni, Cu, W, and Ti) adsorbed on the sidewalls of boron- and nitrogen-doped single-wall carbon nanotubes (B-SWCNTs and N-SWCNTs). The selected TMs have been widely employed in nanoelectronics and nanocatalysis applications, and

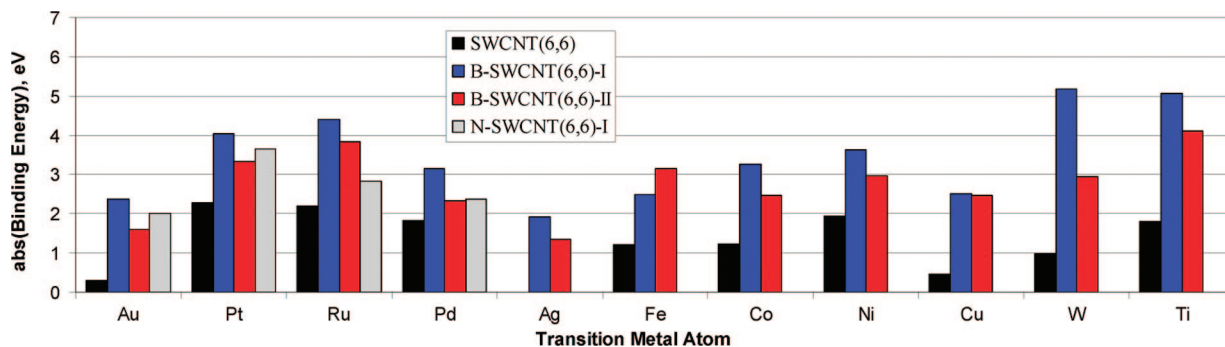


**Figure 4.** Calculated binding energy of the TM atoms on the various SWCNT(6,6) models. The results for the Ti and Au atoms on the pristine SWCNT(6,6) are taken from ref 22.

**TABLE 1: Calculated Minimum Binding Distance (*BD*) of the TM atom to the SWCNT**

structure	TM atom, <i>BD</i> (Å)										
	Au	Pt	Ru	Pd	Ag	Fe	Co	Ni	Cu	W	Ti
TM/B-SWCNT(8,0)-I	2.13	1.91	1.85	2.09	2.17	1.89	1.94	1.91	1.94	1.86	1.95
TM/B-SWCNT(8,0)-II	2.19	2.17	2.16	2.12	2.29	2.02	2.07	2.02	1.98	2.14	2.06
TM/B-SWCNT(6,6)-I	2.05	2.00	1.92	2.04	2.14	1.61	1.81	1.80	1.90	1.77	2.03
TM/B-SWCNT(6,6)-II	2.22	2.27	2.20	2.33	2.27	2.14	2.11	2.08	2.02	1.99	2.20
TM/N-SWCNT(8,0)-I	2.10	1.90	2.01	2.00	-	-	-	-	-	-	-
TM/N-SWCNT(6,6)-I	2.06	1.91	1.91	1.98	-	-	-	-	-	-	-

**TABLE 2: Calculated Magnetic Moment ( $\mu$ )<sup>a</sup> per Supercell of the TM/SWCNT Structures**

structure	TM atom, $\mu(\mu_B)$										
	Au	Pt	Ru	Pd	Ag	Fe	Co	Ni	Cu	W	Ti
isolated TM atom	1	2	4	0	1	4	3	2	1	6	4
TM/B-SWCNT(8,0)-I	0	0	0	0	0	4.2	0	0	0	0.3	0
TM/B-SWCNT(8,0)-II	0	0	1.3	0	0	3.3	1.8	0	0	3.3	1.6
TM/B-SWCNT(6,6)-I	0	0	0	0	0	0	1.9	0	0	0	0
TM/B-SWCNT(6,6)-II	0	0	1.6	0	0	3.3	0	0	0	1.9	1.8
TM/N-SWCNT(8,0)-I	0	0.8	0	0.5	-	-	-	-	-	-	-
TM/N-SWCNT(6,6)-I	0.5	1.4	0.7	1.3	-	-	-	-	-	-	-

<sup>a</sup> Calculated  $\mu$  of isolated B-SWCNT(8,0)-I, N-SWCNT(8,0)-I, B-SWCNT(6,6)-I, N-SWCNT(6,6)-I, B-SWCNT(8,0)-II, and B-SWCNT(6,6)-II per supercell is 0.4, 0.0, 0.3, 0.0, 0.0, and 0.0  $\mu_B$ , respectively.

have high technological interest. Besides the binding configurations and energetics, the effects of doping and TM adsorption on the electronic structure of the SWCNTs are also investigated. Ultimately, these results may serve as a starting point for studying larger, more complex TM nanostructures anchored on the sidewall of boron- or nitrogen-doped CNTs.

## 2. Models and Methods

Two prototype SWCNTs, based on semiconducting SWCNT(8,0) and metallic SWCNT(6,6), were chosen to model B-SWCNTs and N-SWCNTs. In order to explore the effects of the dopant configuration, two distinct models were considered in our study. In the first model, hereafter denoted with an “I”, we explore the maximum expected dopant effect by arranging the dopant atoms in a locally concentrated fashion. In the second model, denoted as “II”, the dopant atoms are arranged more homogeneously (but with the same total concentration) in the SWCNT. In the models, shown in Figure 1, six carbon atoms in the supercell were substituted by B or N atoms, resulting in  $C_{58}B_6$  or  $C_{58}N_6$ , and  $C_{66}B_6$  or  $C_{66}N_6$ , respectively. These approximate concentrations of B-doping ( $B/C \approx 0.1$ ) have been regularly observed in experiments.<sup>24,25</sup> With currently available experimental techniques, only the doping concentration (not the doping pattern) can be controlled. Therefore, our models represent two

idealized cases, which should serve as reference points for analyzing the as-synthesized structures. Both models are structurally stable, with type II structures predicted to have slightly lower total energies. Thus, the dopant arrangements in the type II structures are predicted to be more thermodynamically favorable, while the type I structures are intended to represent more locally concentrated (yet stable) dopant configurations.

The DFT calculations were performed using the Vienna ab initio simulation package (VASP).<sup>31</sup> The program uses a plane-wave basis set, thus offering good access to the Hellmann–Feynman forces acting on all of the atoms in the supercell. Specifically, spin-polarized DFT with the generalized gradient approximation (GGA) of Perdew, Burke, and Ernzerhof (PBE)<sup>32</sup> and the projector-augmented wave (PAW)<sup>33</sup> method were used for the calculations. There are fewer parameters involved in the construction of the PAW potentials, which yields improved accuracy for molecular systems which bear magnetic properties, e.g. transition metals. The PAW technique is essentially an all-electron approach and provides the full wave functions that are not directly accessible with the pseudopotential approach.<sup>34</sup> One-dimensional (1-D) periodic boundary conditions (PBCs) were applied along the tube axis (*c*) to simulate infinitely long nanotube systems. Three unit cells of B(N)-SWCNTs along the

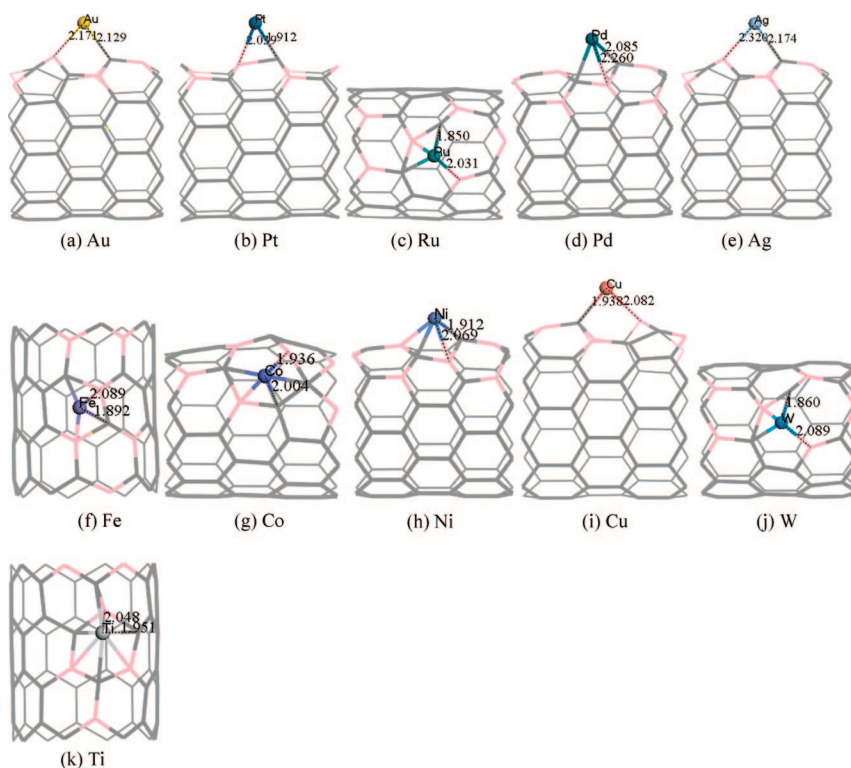


**Figure 5.** Optimized structures of TM/B-SWCNT(8,0)-I within one supercell. The element symbol and shortest binding distance ( $\text{\AA}$ ) between the TM and the nanotube (C and B) are labeled.

*c*-axis were included to build the hexagonal supercell with  $a=b=18\text{\AA}$  and  $a=b=22\text{\AA}$  in the other two directions for B-SWCNT(8,0) and B-SWCNT(6,6), respectively. The separations along the *a* and *b* directions are sufficiently large to avoid interactions between the adsorbed TMs and the images of the nanotubes. A plane wave basis set, truncated with an energy cutoff of 400 eV, was adopted for all of the calculations. The Brillouin-zone of the supercell is sampled by  $1 \times 1 \times 3$  *k*-points with the Monkhorst-Pack scheme,<sup>35</sup> and first-order Methfessel–Paxton smearing<sup>36</sup> of 0.2 eV is employed in the integration. Test calculations have shown that including more *k*-points does not affect the results. The positions of all of the atoms in the supercell were fully relaxed during the geometry optimizations. The convergence threshold was set to be  $10^{-4}$  eV for the total energy in the electronic self-consistent-loop and  $10^{-2}$  eV/ $\text{\AA}$  of force on each atom. On the basis of the equilibrium structures,  $1 \times 1 \times 10$  *k*-points were then used to compute the electronic structures. In test calculations, additional *k*-points did not alter the electronic structure results.

We examined a number of different binding sites (close to the doping sites) on the sidewalls of B-SWCNTs and N-SWCNTs for the TM adsorption. For example, we chose the top (above the B, N, or C atom), bridge (above the B–C, N–C, or C–C bond), and hollow (above the  $(\text{BC})_3$ ,  $(\text{NC})_3$ ,  $\text{B}_2\text{C}_4$ , or  $\text{N}_2\text{C}_4$  or  $\text{BC}_5$  hexagon) site in order to locate the lowest-energy configuration for the adsorbate/adsorbent system. Given the wide variety of adsorption sites available in our models, the maximum and minimum effects of doping on the TM adsorption should be sufficiently sampled in our study. The binding energy reported in this study is defined as  $BE = E_{\text{total}}(\text{tube} + \text{TM}) - E_{\text{total}}(\text{tube}) - E_{\text{total}}(\text{TM})$ , where  $E_{\text{total}}$  is the total energy of the system per supercell. Hence, negative (positive)  $BE$  denotes an exothermic (endothermic) binding process.

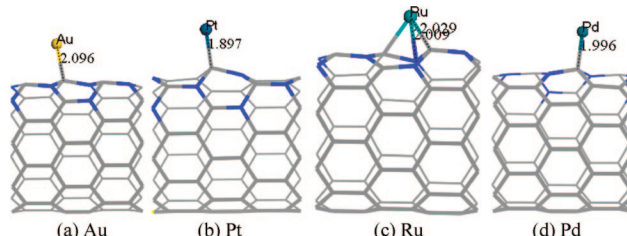


**Figure 6.** Optimized structures of TM/N-SWCNT(8,0)-I within one supercell. The element symbol and shortest binding distance ( $\text{\AA}$ ) between the TM and the nanotube (C and N) are labeled.

### 3. Results and Discussion

**3.1. Geometric and Electronic Structures of Isolated SWCNTs.** Our calculations show that the pristine SWCNT cross-section is changed from round to a slightly elongated ellipse after boron doping, while it is changed to a “water drop” shape after nitrogen doping (Figure 1). The diameters of the B-SWCNTs are slightly enlarged by 5–7%, as compared to those of the corresponding pristine SWCNTs, but the overall geometry of the SWCNTs remains intact after doping. The lack of any major distortions in B-SWCNT is expected because there is a deficiency of electrons after boron doping. Therefore, there are no occupied lone-pair orbitals present at the adjacent C atoms, similar to the case in the unsubstituted SWCNTs. However, the incorporation of N atoms into the SWCNTs results in more drastic curvature, with a much larger maximum diameter (enlarged by 11–14%). The increased curvature could be due to the electron-rich nature of the nitrogen dopant compared to the carbon host, leading to a more tetrahedral coordination of the adjacent C atoms with the lone-pair electrons.<sup>37</sup> As expected, the energy cost of forming N-SWCNTs will be higher than that of forming B-SWCNTs. Indeed, the formation energy (defined as  $E_{\text{form}} = (E_{\text{total}}(\text{doped}) - \text{SWCNT}) + nE_C - E_{\text{total}}(\text{SWCNT})$  –

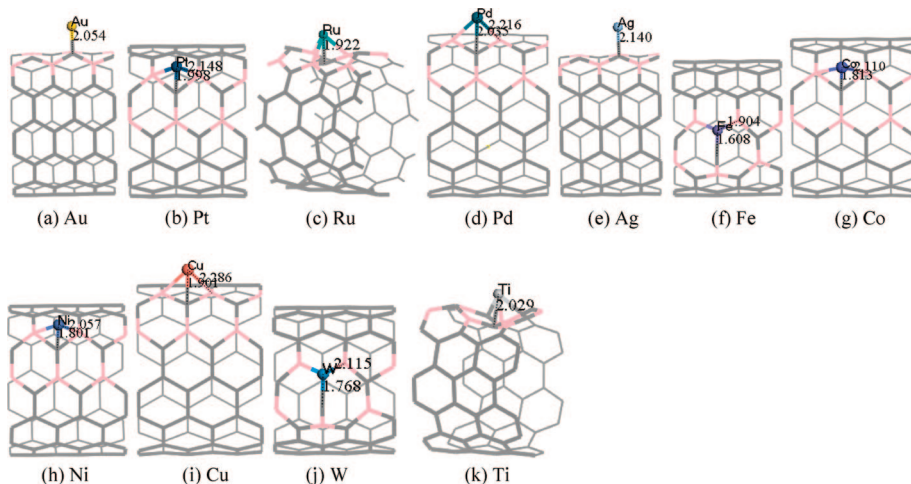


**Figure 7.** Optimized structures of TM/B-SWCNT(6,6)-I within one supercell, as in Figure 5.

$nE_B)/n$ , where  $n$  is the number of carbon atoms substituted) of N-SWCNTs is 3.67 and 3.78 eV for the (8,0) and (6,6) nanotubes, respectively, compared to those of the corresponding B-SWCNTs (2.59 and 2.50 eV). Due to less geometrical strain, the evenly doped SWCNTs (type II) are expected to have lower total energy per supercell than those of the unevenly doped ones (type I), i.e.,  $-1.58$  eV for B-SWCNT(8,0)-II and  $-0.03$  eV for B-SWCNT(6,6)-II. Note that B-SWCNT(6,6)-I and -II are almost isoenergetic due to larger diameter of pristine SWCNT(6,6). Therefore, it is expected that the energy difference in these two models will be decreased as larger-sized SWCNTs or MWCNTs are employed for doping.

Only N-doped SWCNTs with type I structures were explored. In contrast to the B-doped models, the results from the N-doped models were less substantial, so only the locally concentrated dopant configuration (type I) was investigated with nitrogen. Thus, we expect the results for the type I model to represent a reasonable upper limit for the N-doped SWCNTs (in terms of the enhanced binding energy), similar to the results from the B-doped SWCNTs.

Calculated band structures and density of states (DOS) show that the electronic properties of the SWCNTs can be modified by either *p*-type boron or *n*-type nitrogen doping (Figure 2). The SWCNT(8,0) model is semiconducting, with a direct band gap of  $\sim 0.6$  eV, while SWCNT(6,6) is metallic, with the valence and conduction bands contacting at the Fermi level. After locally concentrated boron doping (type I structure), the gap of pristine SWCNT(8,0) becomes filled mainly by *2p*-states of carbon and boron where the Fermi level lies. The induced acceptor-type state is clearly seen above the valence band (VB) maximum of the original pristine SWCNT(8,0). The semiconducting SWCNT(8,0) is therefore turned into a metallic nanotube with *p*-type conduction by boron doping, and weak spin states are even created, due mainly to carbon *2p*-states, consistent with a previous report on SWCNT(16,0).<sup>38</sup> For B-SWCNT(6,6)-I, the Fermi level is pulled down into the VB of the pristine SWCNT(6,6), where more electronic states are located. One spin-down electron channel is visible at the VB maximum. Therefore, SWCNTs can be tuned to function as metallic nanowires by locally concentrated boron doping, regardless of the inherent conductivity of the pristine SWCNTs. In contrast, induced donor-type states are created below the conduction band (CB) minimum of the pristine SWCNT(8,0) due to nitrogen doping, and cross the Fermi level of N-SWCNT(8,0)-I. Hence,

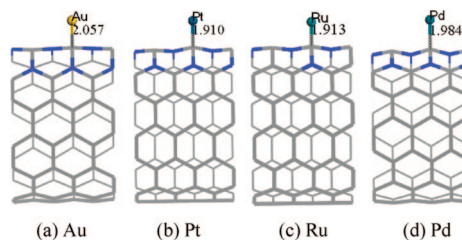


**Figure 8.** Optimized structures of TM/N-SWCNT(6,6)-I within one supercell, as in Figure 6.

the semiconducting SWCNT(8,0) is tuned to become a metallic nanotube with *n*-type conduction by nitrogen doping. This agrees with a previous experimental and modeling study of N-SWCNT(17,0), in which the N dopants were arranged randomly and homogeneously in a pyridine-like configuration.<sup>39</sup> Interestingly, N-SWCNT(6,6)-I becomes semiconducting because a small gap is reopened in the small energy regime near the Fermi level, due to the strong interaction of the *p*-state of nitrogen and carbon at the VB maximum and CB minimum (see *p*-DOS in Figure 2f). The enhanced curvature effect induced by the nitrogen dopant also plays a role in modifying the electronic structure of SWCNT(6,6).<sup>40</sup> Several experimental studies<sup>41,42</sup> have reported on the application of nitrogen-doped multiwalled carbon nanotubes (MWCNTs) as *n*-type FETs, indicating the feasibility of using doped CNTs with semiconducting features. Surprisingly, the type II B-SWCNT models show no magnetism at all. The electronic structures resemble those of the corresponding pristine SWCNTs except that the Fermi level is lowered down into the valence band, making them all metallic in nature (Figure 2, parts g and h). In general, our electronic structure calculations agree well with the experimental findings that boron and nitrogen-doped CNTs are *p*- and *n*-type conductors, respectively.<sup>43</sup>

**3.2. TM Chemisorption on B- and N-SWCNTs: Energetics and Binding Configurations.** A similar systematic study on the adsorption of individual atoms on pristine SWCNT(8,0) and (6,6) has been recently reported.<sup>22</sup> Durgun et al. have shown that most of the TM adatoms are chemisorbed on the sidewall of SWCNTs based on spin-restricted DFT calculations, but if spin-polarized calculations are used, then the adsorption is found to be a weaker chemisorption or a van der Waals-type interaction. Because most TM atoms are in a magnetic ground state, and the magnitude of the binding energy (*BE*) is directly

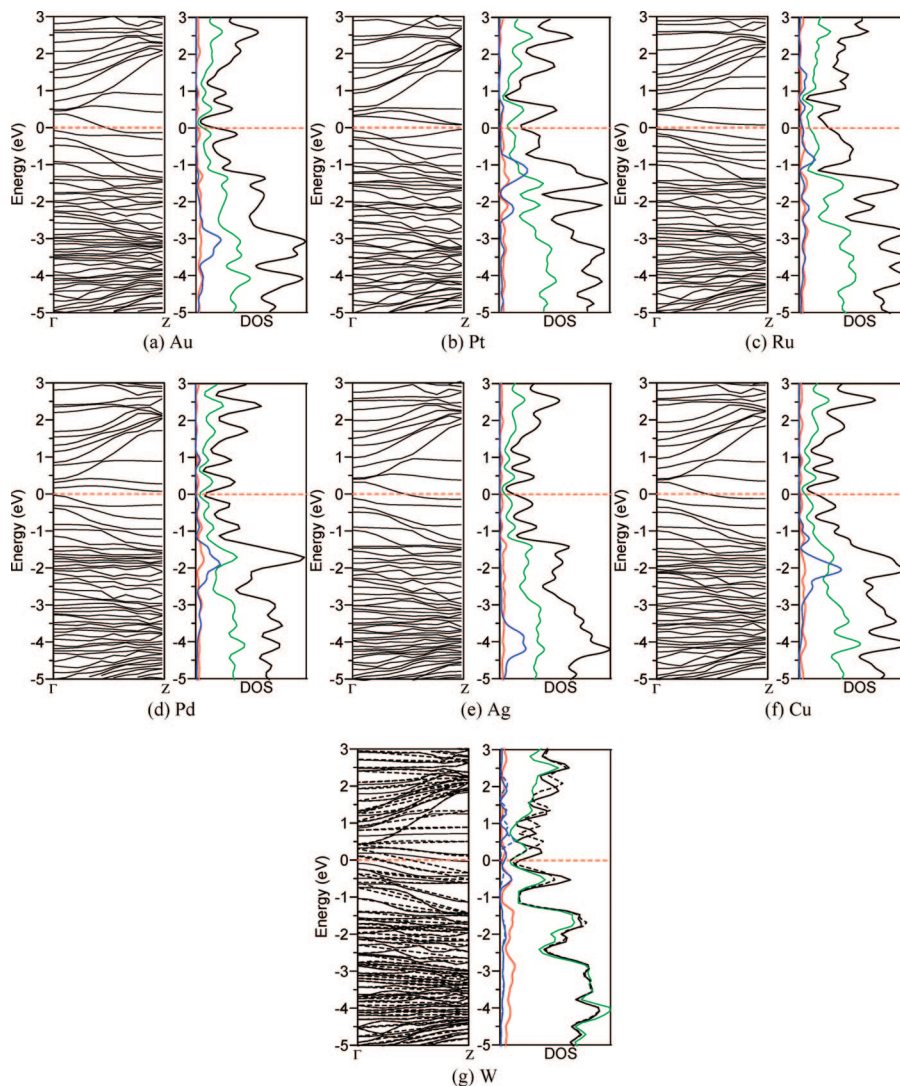


**Figure 9.** Calculated band structure and density of states (DOS) for the TM/B-SWCNT(8,0)-I system, as in Figure 2. Blue represents the projected TM *d*-state.

dependent on the accuracy of the total energy of the constituent and final combined systems, we exclusively used spin-polarized DFT calculations in this study. Also, a similar study of 3d TM atoms adsorbed on a boron nitride (BN) nanotube (8,0) model was reported by Wu et al.<sup>44</sup> A similar trend of 3d TM binding energies was obtained between BNNT (8,0) and SWCNT (8,0). These materials have the same *sp*<sup>2</sup> bonding scheme, similar curvature, and certain similarities in their electronic structure, i.e., semiconducting. As is known, all BNNTs are wide band gap semiconductors, independent of chirality. It should also be noted that although B and N are the dopant elements studied in our work, they are only present in low concentrations, as compared to BNNTs. Thus, our calculated TM *BEs* on the doped SWCNTs are mainly compared to the previous spin-polarized results on pristine SWCNTs by Durgun, et al.,<sup>22</sup> as shown in Figures 3 and 4. The numerical values are listed in Table S1 in the Supporting Information. Also, the binding distance (*BD*) and magnetic moment ( $\mu$ ) per supercell are collected in Tables 1 and 2. We expect that the results from the locally concentrated doping (type I models) will yield the maximum effects on the TM adsorption, while the type II models are expected to indicate the effects of a more random dopant distribution. Therefore, the results from the type II models are likely to be more representative of the effects attainable with current doping

techniques. The underlying chemical binding trends that we predict should also hold for similar B- and N-doped SWCNTs or MWCNTs.

**3.2.1. TM/B-SWCNT(8,0)-I and TM/N-SWCNT(8,0)-I.** As shown in Figure 5, the lowest-energy configurations of TM/B-SWCNT(8,0)-I can be characterized as forming multiple TM-C and TM-B bonds at the hollow sites containing B atoms. In contrast, the TM atoms in TM/N-SWCNT(8,0)-I are chemisorbed on top of the C atoms bonded with N atoms (Figure 6), except the Ru atom, which is chemisorbed at the hollow site with multiple TM-C and TM-N bonds formed. In general, boron doping leads to significantly enhanced binding of TM atoms, compared to that on pristine SWCNTs (see Figure 3). For instance, the BEs for Au, Pt, and Pd atoms adsorbed on B-SWCNT(8,0)-I are increased to -3.35, -4.03, and -3.58 eV from -0.5, -2.4, and -1.7 eV on pristine SWCNT(8,0), respectively. Nitrogen doping also leads to moderate enhancements in BEs, e.g., -1.55 and -2.90 eV for Au and Pt adsorbed on N-SWCNT(8,0)-I, respectively. It can be seen that B doping is more effective for enhancing the binding of TMs than N doping. Thus, we performed additional calculations for other TM atoms adsorbed on B-doped SWCNTs, and we also explored other B-doping arrangements (type II). Indeed, the enhanced binding due to incorporation of boron can be observed for all

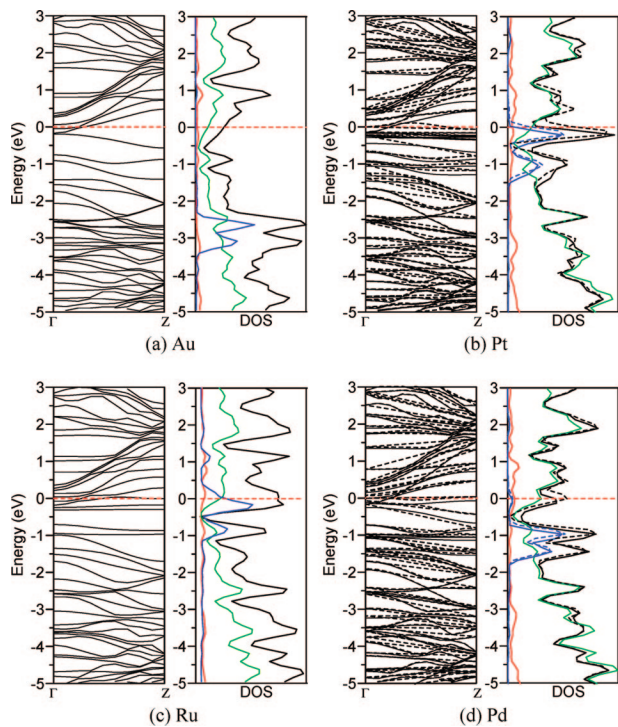


**Figure 10.** Calculated band structure and density of states (DOS) for the TM/N-SWCNT(8,0)-I system, as in Figure 9.

TMs studied here, e.g., the BEs for Fe, W, and Ti atom are increased from  $-0.8$ ,  $-0.9$ , and  $-2.2$  eV to  $-4.17$ ,  $-6.43$ , and  $-6.82$  eV on B-SWCNT(8,0)-I, respectively. The enhanced chemisorption is evident from the magnitude of the BEs and shorter BDs (Table 1), as compared to the adsorption of the same TM atoms on pristine SWCNTs.<sup>22</sup> In addition, the increasing trend in BEs holds for all TMs, regardless of the presence of either strong or weak magnetism in the free atoms.

It is known that the magnetism of a nanostructural material is mainly attributed to the intrinsic spin-magnetic moment of the individual atoms, while it is reduced by the formation of chemical bonds and the kinetic energy of electrons, which can even quench the spin magnetization in the bulk material. Due to enhanced binding, all of the TMs are expected to form continuous or quasi-continuous coating at the B- or N-doping sites. Considering that CNTs can function as a template for growing TM nanostructures, if magnetic properties can be stabilized by either B- or N-CNTs, there may be applications in nanomagnetic and spintronic applications.<sup>45,46</sup> However, as shown in Table 2, the spin-magnetic moment ( $\mu$ ) of the individual TM atoms is quenched to zero for almost all TMs (except Fe and W) upon their chemisorptions on B-SWCNT(8,0)-I. In comparison, the isolated B-doped SWCNT supports become weakly magnetic when doped:  $0.4$  and  $0.3 \mu_B$  for B-SWCNT(8,0)-I and B-SWCNT(6,6)-I, respectively. This behavior is in stark contrast to the adsorption of TMs on pristine SWCNTs, which are nonmagnetic but considerable  $\mu$  is retained for the TM/SWCNT composite.<sup>22</sup> Formation of multiple chemical bonds between the TM atoms and the doped SWCNTs could play a key role in quenching the inherent magnetism originating from the free TM atoms. In the cases where TM = Fe and W, TM/B-SWCNT(8,0)-I has a  $\mu$  of  $4.2$  and  $0.3 \mu_B$ , respectively. Due to its weak magnetism ( $0.4 \mu_B$  per supercell), B-SWCNT(8,0)-I may partly contribute to the spin-magnetic moment of Fe/B-SWCNT(8,0)-I. However, TM/N-SWCNT(8,0)-I with TM = Pt and Pd, show weak magnetism with  $\mu$  less than  $1 \mu_B$ .

Because our supercell models contained a single TM atom and gas-phase TM atoms are known to be highly reactive, the BEs calculated in this study can serve as an upper limit, with respect to more realistic TM NPs or other nanostructures (e.g., nanochains or films) adsorbed on B- or N-CNTs. Likewise, the calculated  $\mu$  of our combined TM/B-SWCNT or TMN-SWCNT structures can be treated only as a guideline for more realistic nanostructures because  $\mu$  critically depends on the binding state of the TMs, in which cases TM–TM interactions (adatom-adatom) may impart significant effects. Also, thermal effects are currently nonexistent in our calculations.

**3.2.2. TM/B-SWCNT(6,6)-I and TM/N-SWCNT(6,6)-I.** As shown in Figure 4, both B-SWCNT(6,6)-I and N-SWCNT(6,6)-I also show enhanced binding with TM atoms, as compared to pristine SWCNT(6,6). However, the magnitude of the enhancement is lower, possibly due to the reduced curvature in B(N)-SWCNT(6,6)-I as compared to that of B(N)-SWCNT(8,0)-I, suggesting that the local geometric strain also plays a key role in the reactivity of the tube-like structure.<sup>47</sup> From Figures 7 and 8, it can be seen that the TM atoms prefer to chemisorb on the top site (when TM = Au, Ru, Ag, Fe, W, or Ti), or close to the top site (when TM = Pt, Pd, Co, Ni, or Cu), of the C atom bonded with B or N atoms in B(N)-SWCNT(6,6)-I. This result is in contrast to TM/B-SWCNT(8,0)-I, where the hollow sites are the most favorable adsorption sites. In terms of the magnetic properties, the TM/B-SWCNT(6,6)-I composite becomes non-magnetic upon the chemisorption of the TMs, except for the Co atom with  $\mu = 1.9 \mu_B$ , which is consistent with the experimentally observed magnetism of single Co atoms, NPs, and nanochains anchored on the metallic substrates Pt(997) and Pt(111).<sup>45,48</sup> As in TM/N-SWCNT(8,0)-I, Au, Pt, and Pd, as well as Ru atoms, are chemisorbed on top of the C atom of the C–N bond, generating weak magnetism ranging from  $0.5$  to  $1.4 \mu_B$ .

**3.2.3. TM/B-SWCNT(8,0)-II and TM/B-SWCNT(6,6)-II.** The results of TM adsorption on the type II models are included in Tables 1 and 2, Figures 3 and 4, and in the Supporting Information. The BEs for the TMs are predicted to be smaller than those of the corresponding TMs on the type I B-SWCNT models. However, boron-doping in a more dispersed manner is still found to greatly enhance the TM binding strength, as compared to the pristine SWCNTs. In comparison, the difference in BEs caused by different doping patterns in the SWCNTs is found to be much larger than that of boron-doped graphene models.<sup>49</sup> As is known, graphene is a flat sheet of carbon in a hexagonal lattice, and SWCNTs can be viewed as tubular structures which are constructed by seamlessly rolling up a graphene sheet along certain directions. As a consequence, the geometric stain inherent to SWCNTs is much larger than graphene, leading to slight differences in their  $sp^2$  bonding, i.e., deviating from the true  $sp^2$  bonding in graphene. Moreover, the nanoscale tubular geometry imparts unique electronic structures to SWCNTs, which can be metallic or semiconductive. This is due to the quantization of electron waves along the circumference of the tube (depending upon the chirality), whereas larger-scale graphene has uniform electronic properties, i.e., conducting. It is therefore expected that SWCNTs are more sensitive to the doping pattern than graphene, which ultimately renders more dramatic effects on the adsorption characteristics.

It should be noted that the type I and type II models employed in this study represent two feasible benchmarks for the doping patterns. Clearly, locally concentrated enrichment of boron within the CNTs will enhance the TM binding strength more than the sparsely substituted boron. It is expected that the magnitude of the BEs in reality will be within the range of our

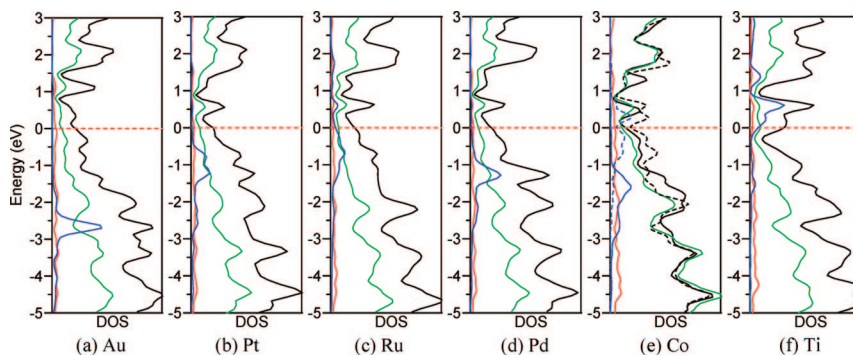


**Figure 11.** Calculated density of states (DOS) for the TM/B-SWCNT(6,6)-I system, as in Figure 9.

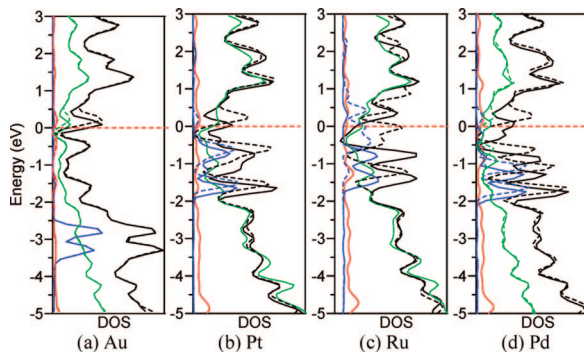


**Figure 12.** Calculated density of states (DOS) for the TM/N-SWCNT(6,6)-I system, as in Figure 9.

calculated type II model results, considering the irregular doping patterns currently attainable in experimental synthesis.

**3.3. TM Atom Chemisorption on B- and N-SWCNTs: electronic structure.** When used as a component material in a specific application (nanoelectronics, nanocatalysis, spintronics, sensors, etc.), TM/B-SWCNT or TM/N-SWCNTs should have a suitable electronic structure. Tuning the electronic structure of the B(N)-SWCNT by the TM nanostructure or vice versa is a key issue for practical applications. Band structure and density of states (DOS) calculations are both used to analyze the modifications of the electronic structure. According to the supercell method with PBCs, the calculated band structures in this study correspond to the energy states of a geometry with a periodic “chain” of TM-adatoms anchored on B(N)-SWCNT. As mentioned in Section 2, the interatomic separation between TM-adatoms in the periodic system along the *c* direction is equivalent to  $3 \times$  the lattice parameter of B(N)-SWCNT, which is sufficiently large to avoid effects from any adatom-adatom interaction.

**3.3.1. TM/B-SWCNT(8,0) and TM/N-SWCNT(8,0).** As shown in Figure 9, due to a *single* TM atom included in the model, the electronic structures of TM/B-SWCNT(8,0)-I demonstrate a variety of characteristics, while the overall features of the B-SWCNTs are retained. As mentioned above, B-SWCNTs are tuned to be metallic by locally concentrated B doping. In contrast, TM/B-SWCNT(8,0)-I becomes less metallic upon chemisorption of the TM atoms because fewer states are retained at the Fermi level, as compared to those of B-SWCNT(8,0)-I. From the projected-DOS, it can be seen that the chemical bonding between the TM atoms and the sidewall of B-SWCNT(8,0)-I is mainly attributed to the interaction between the 2*p*-states of C and B and the *d*-states of the TM atom, which occurs in the region below the Fermi level (0 to  $\sim$ 5 eV). Furthermore, our calculations predict that the *s*-states of C, B, and the TMs

contribute almost nothing to the interaction between the TMs and the SWCNTs, within the energy range of  $-5\text{--}3$  eV. As such, some of the 2*p*-states of C and B at the Fermi level are pulled down by the *d*-states of the TM, while the position of overlap varies among the different TM atoms. For example, for TM/B-SWCNT(8,0)-I with TM = Au, Pt, Ru, Pd, Ag, Cu, and W, the maximum overlap occurs at  $\sim$ −3.0, −1.2, −0.8, −1.9, −4.1, −2.1, and −0.5 eV below the Fermi level, respectively.

It can be seen that a single band crossing the Fermi level is contributed from the electronic states of C and B, as shown in the *p*-DOS plots in Figure 9, parts a, e, and f, of TM/B-SWCNT(8,0)-I, with TM = Au, Ag, and Cu having  $(n-1)d^{10}ns^1$  valence electronic configurations with closed *d* shells. By contrast, a tiny indirect gap seems almost reopened for TM/B-SWCNT(8,0)-I with TM = Pt, Ru, or Pd. Furthermore, spin-polarized states of TM/B-SWCNT(8,0)-I are mainly attributed to the *d*-spin states of the TM, as shown in Figure 9g for W/B-SWCNT(8,0)-I with  $\mu = 0.3 \mu_B$ . Note that the BEs for Au, Ag, and Cu are smaller in magnitude, as compared to those for the other TMs. The difference in the band shape around the Fermi level is apparently affected by the chemical bonding of the TM atom with the nanotube, leading to different electronic properties of the TM/B-SWCNT(8,0)-I composite. In contrast to the result that most of the TM/B-SWCNT(8,0)-I composites are nonmagnetic, the TM/B-SWCNT(8,0)-II structures, where TM = Ru, Fe, Co, W, and Ti, are magnetic (Table 2). This result arises from a combination of the magnetism of the TM atoms and the nonmagnetism of the uniformly doped-SWCNTs. Therefore, the electronic structure of the substrate nanotubes can be tailored by carefully selecting the TMs or the doping pattern, if possible.

Likewise, the electronic properties of N-SWCNT(8,0)-I can be modified by chemisorption of TM atoms, as shown in Figure 10. The significant change in band shape and distribution of states can be found for TM/N-SWCNT(8,0)-I with TM = Pt, Ru, and Pd. Clearly, these changes arise from extra *d*-states of the TM-adatom and the consequent electronic resonance with the 2*p*-states of C and N. Unlike TM/B-SWCNT(8,0)-I, the *d*-states of Pt and Ru also contribute partly to the electronic state at the Fermi level, which leads to the enhanced conductivity of the TM/N-SWCNT(8,0)-I system. In addition, because isolated N-SWCNT(8,0)-I is nonmagnetic, the *d*-spin states of the TM (TM = Pt or Pd) adatom are expected to solely give rise to the magnetism of the TM/N-SWCNT(8,0)-I system, as shown in Figure 10, parts b and d.

**3.3.2. TM/B-SWCNT(6,6) and TM/N-SWCNT(6,6).** As in TM/B(N)-SWCNT(8,0), the electronic structure of B(N)-SWCNT(6,6) is built upon that of pristine SWCNT(6,6), which determines the main DOS features, as shown in Figures 11 and

12. Similarly, the interaction between the *d*-states of the TM and the *2p*-states of C and B(N) is mainly responsible for the chemical bonding of the TM atom with the doped SWCNTs. The DOS is varied with chemisorbed TM adatoms, whose *d*-states generate electronic resonance with the *2p*-states of C and B(N) at different energy levels. For example, the *d*-states of Au, Pt, and Pd do not contribute to the conductivity of TM/B-SWCNT(6,6)-I, whereas Ru, Co, and Ti atoms generate electronic states at the Fermi level. In particular, the *d*-spin states of Co around the Fermi level result in the magnetism of Co/B-SWCNT(6,6)-I, as shown in Figure 11e. In general, the metallic nature of B-SWCNT(6,6)-I remains unchanged upon the chemisorption of TM atoms. Similar to TM/B-SWCNT(8,0)-II, TM/B-SWCNT(6,6)-II, where TM = Ru, Fe, W, and Ti, are found to be magnetic (Table 2). Therefore, the magnetism of the TM and the substrate both have an impact on the magnetic properties of TM/doped-SWCNT composite.

For N-SWCNT(6,6)-I, the chemisorbed Au, Pt, Ru, and Pd atoms can convert the substrate from an initial nonmagnetic into a magnetic nanostructure. Moreover, the small gap of N-SWCNT(6,6)-I becomes connected, due to either the uplift of the Fermi level or to the new states created by the TM-adatoms. The magnetism of TM/N-SWCNT(6,6)-I is attributed to both the *d*-spin states of the TM and to the induced *2p*-spin states of carbon, as shown in Figure 12.

#### 4. Conclusions

We have systematically investigated the adsorption of eleven technologically relevant TMs, i.e., Au, Pt, Ru, Pd, Ag, Fe, Co, Ni, Cu, W, and Ti, on both B-doped and N-doped SWCNT(8,0) and (6,6) models. Our spin-polarized DFT calculations show that (1) locally concentrated nitrogen doping creates more geometric strain in SWCNTs than that of boron doping, leading to a larger energy cost of formation; (2) the *p*-type boron doping leads to conductive SWCNTs regardless of the inherent conductivity of the pristine SWCNTs being semiconducting or metallic, whereas the *n*-type nitrogen doping leads to conductive N-SWCNT(8,0) but slightly semiconducting N-SWCNT(6,6); (3) either B- or N-doped SWCNTs can lead to enhanced binding, i.e., chemisorption, with individual TM atoms, as compared to adsorption of the same TM atoms on pristine SWCNTs; (4) comparatively, boron doping results in greater enhancement of TM binding strength than nitrogen doping; (5) the chemical bonding of TM atoms with the sidewall of B- or N-doped SWCNTs is mainly attributed to the interaction between the *2p*-states of C and B/N and the *d*-states of the TM; (6) the doping pattern has an impact on the magnetism of the doped-SWCNTs, and the magnetism of individual TM atoms is quenched or reduced when chemisorbed on B-doped SWCNTs. The magnetism of TM/doped-SWCNT is mainly contributed from the TM but is also dependent upon the magnetism of the substrate; and (7) although the overall electronic structure features of the doped SWCNTs are retained, due to the chemisorption of a single TM atom, the electronic properties of the TM/B-SWCNT systems can be tuned, which leaves room for tailoring TM/B(N)-CNT composites for specific applications.

**Acknowledgment.** Funding for this work was provided by an NSF CAREER Award (no. 0747690). Supercomputer resources were provided by the Alabama Supercomputer Center, NCSA TeraGrid, and the Pacific Northwest National Laboratory EMSL facility.

**Supporting Information Available:** Table of (1) calculated binding energy (*BE*) of the TM atoms to the SWCNT; (2)

calculated binding distance (*BD*) of TM atoms to the atom sites on B-SWCNT-II; (3) calculated binding distance (*BD*) and spin-magnetic moment (*μ*) of TM atoms adsorbed on pristine SWCNT (6,6). Figures of (1) optimized structures of TM/B-SWCNT(8,0)-II within one supercell; and (2) optimized structures of TM/B-SWCNT(6,6)-II within one supercell. This material is available free of charge via the Internet at <http://pubs.acs.org>.

#### References and Notes

- (1) (a) Iijima, S. *Nature* **1991**, *354*, 56. (b) Iijima, S.; Ichihashi, T. *Nature* **1993**, *363*, 603.
- (2) Thess, A.; Lee, R.; Nikolaev, P.; Dai, H.; Petit, P.; Robert, J.; Xu, C.; Lee, Y. H.; Kim, S. G.; Rinzler, A. G.; Colbert, D. T.; Scuseria, G. E.; Tománek, D.; Fischer, J. E.; Smalley, R. E. *Science* **1996**, *273*, 483.
- (3) Wildöer, J. W. G.; Venema, L. C.; Rinzler, A. G.; Smalley, R. E.; Dekker, C. *Nature* **1998**, *391*, 59.
- (4) Odom, T. W.; Huang, J. L.; Kim, P.; Lieber, C. M. *Nature* **1998**, *391*, 62.
- (5) Bethune, D. S.; Klang, C. H.; de Vries, M. S.; Gorman, G.; Savoy, R.; Vazquez, J.; Beyers, R. *Nature* **1993**, *363*, 605.
- (6) Avouris, P.; Chen, J. *Mater. Today* **2006**, *9*, 46.
- (7) Sahoo, S.; Kontos, T.; Furer, J.; Hoffmann, C.; Gruber, M.; Cottet, A.; Schonenberger, C. *Nat. Phys.* **2005**, *1*, 99.
- (8) Planeix, J. M.; Coustel, N.; Coq, J.; Brotons, V.; Kumbhar, P. S.; Dutarte, R.; Geneste, P.; Bernier, P.; Ajayan, P. M. *J. Am. Chem. Soc.* **1994**, *116*, 7935.
- (9) Kongkanand, A.; Kuwabata, S.; Girishkumar, G.; Kamat, P. *Langmuir* **2006**, *22*, 2392.
- (10) Kong, J.; Franklin, N. R.; Zhou, C.; Chapline, M. G.; Peng, S.; Cho, K.; Dai, H. *Science* **2000**, *287*, 622.
- (11) Baughman, R. H.; Zakhidov, A. A.; de Heer, W. A. *Science* **2002**, *297*, 787.
- (12) See a special issue on carbon nanotubes in the following: *Acc. Chem. Res.* **2002**, *35*, 997.
- (13) Javey, A. *ACS Nano* **2008**, *2*, 1329.
- (14) Georgakilas, V.; Gournis, D.; Tzitzios, V.; Pasquato, L.; Guldi, D. M.; Prato, M. *J. Mater. Chem.* **2007**, *17*, 2679.
- (15) Tans, S. J.; Verschueren, R. M.; Dekker, C. *Nature* **1998**, *393*, 49.
- (16) Collins, P. G.; Arnold, M. S.; Avouris, P. *Science* **2001**, *292*, 706.
- (17) Bachtold, A.; Hadley, P.; Nakanishi, T.; Dekker, C. *Science* **2001**, *294*, 1317.
- (18) Keren, K.; Berman, R. S.; Buchstab, E.; Sivan, U.; Braun, E. *Science* **2003**, *302*, 1380.
- (19) Guo, X. F.; Small, J. P.; Klare, J. E.; Wang, Y.; Purewal, M. S.; Tam, I. W.; Hong, B. H.; Caldwell, R.; Huang, L.; O'Brien, S.; Yan, J.; Breslow, R.; Wind, S. J.; Hone, J.; Kim, P.; Nuckolls, C. *Science* **2006**, *311*, 356.
- (20) Qi, P.; Javey, A.; Rolandi, M.; Wang, Q.; Yenilmez, E.; Dai, H. J. *J. Am. Chem. Soc.* **2004**, *126*, 11774.
- (21) Wei, D.; Liu, Y.; Cao, L.; Wang, Y.; Zhang, H.; Yu, G. *Nano Lett.* **2008**, *8*, 1625.
- (22) Durgun, E.; Dag, S.; Ciraci, S.; Gulseren, O. *J. Phys. Chem. B* **2004**, *108*, 575, see spin-polarized calculation results.
- (23) Stéphan, O.; Ajayan, P. M.; Colliex, C.; Redlich, P.; Lambert, J. M.; Bernier, P.; Lefin, P. *Science* **1994**, *266*, 1683.
- (24) Han, W.; Bando, Y.; Kurashima, K.; Sato, T. *Chem. Phys. Lett.* **1999**, *299*, 368.
- (25) (a) Golberg, D.; Bando, Y.; Han, W.; Kurashima, K.; Sato, T. *Chem. Phys. Lett.* **1999**, *308*, 337. (b) Golberg, D.; Bando, Y.; Bourgeois, L.; Kurashima, K.; Sato, T. *Carbon* **2000**, *38*, 2017.
- (26) Gai, P. L.; Stéphan, O.; McGuire, K.; Rao, A. M.; Dresselhaus, G.; Dresselhaus, M. S.; Colliex, C. *J. Mater. Chem.* **2004**, *14*, 669.
- (27) Wei, B.; Spolenak, R.; Kohler-Redlich, P.; Rühle, M.; Arzt, E. *Appl. Phys. Lett.* **1999**, *74*, 3149.
- (28) Charlier, J. C.; Terrones, M.; Baxendale, M.; Meunier, V.; Zacharia, T.; Rupasinghe, N. L.; Hsu, W. K.; Grobert, N.; Terrones, H.; Amaralunga, G. A. J. *Nano Lett.* **2002**, *2*, 1191.
- (29) Carroll, D. L.; Redlich, P.; Blase, X.; Charlier, J.-C.; Curran, S.; Ajayan, P. M.; Roth, S.; Rühle, M. *Phys. Rev. Lett.* **1998**, *81*, 2332.
- (30) Acharya, C. K.; Turner, C. H. *J. Phys. Chem. B* **2006**, *110*, 17706.
- (31) (a) Kresse, G.; Hafner, J. *Phys. Rev. B* **1993**, *47*, 558. (b) Kresse, G.; Furthmüller, J. *Comput. Mater. Sci.* **1996**, *6*, 15. (c) Kresse, G.; Furthmüller, J. *Phys. Rev. B* **1996**, *54*, 11169.
- (32) Perdew, J. P.; Burke, K.; Ernzerhof, M. *Phys. Rev. Lett.* **1996**, *77*, 3865.
- (33) Blöchl, P. E. *Phys. Rev. B* **1994**, *50*, 17953. (b) Kresse, G.; Joubert, D. *Phys. Rev. B* **1999**, *59*, 1758.
- (34) Hobbs, D.; Hafner, J.; Spišák, D. *Phys. Rev. B* **2003**, *68*, 014407.
- (35) Monkhorst, H. J.; Pack, J. D. *Phys. Rev. B* **1976**, *13*, 5188.

- (36) Methfessel, M.; Paxton, A. *Phys. Rev. B* **1989**, *40*, 3616.
- (37) Sidik, R. A.; Anderson, A. B.; Subramanian, N. P.; Kumaraguru, S. P.; Popov, B. N. *J. Phys. Chem. B* **2006**, *110*, 1787.
- (38) Fuentes, G. G.; Borowiak-Palen, E.; Knupfer, M.; Pichler, T.; Fink, J.; Wirtz, L.; Rubio, A. *Phys. Rev. B* **2004**, *69*, 245403.
- (39) Czerw, R.; Terrones, M.; Charlier, J. C.; Blase, X.; Foley, B.; Kamalakaran, R.; Grobert, N.; Terrones, H.; Ajayan, P. M.; Blau, W.; Tekleab, D.; Rühle, M.; Carroll, D. L. *Nano Lett.* **2001**, *1*, 457.
- (40) Crespi, V. H.; Cohen, M. L.; Rubio, A. *Phys. Rev. Lett.* **1997**, *79*, 2093.
- (41) Xiao, K.; Liu, Y. Q.; Hu, P. A.; Yu, G.; Sun, Y. M.; Zhu, D. B. *J. Am. Chem. Soc.* **2005**, *127*, 8614.
- (42) Zhang, W. J.; Zhang, J. Y.; Li, P. J.; Shen, X.; Zhang, Q. F.; Wu, J. L. *Nanotechnology* **2008**, *19*, 085202.
- (43) Choi, Y. M.; Lee, D. S.; Czerw, R.; Chiu, P. M.; Grobert, N.; Terrones, M.; Reyes-Reyes, M.; Terrones, H.; Charlier, J. C.; Ajayan, P. M.; Roth, S.; Carroll, D. L.; Park, Y. W. *Nano Lett.* **2003**, *3*, 839.
- (44) Wu, X. J.; Zeng, X. C. *J. Chem. Phys.* **2006**, *125*, 044711.
- (45) Gambardella, P.; Rusponi, S.; Veronese, M.; Dhesi, S. S.; Grazioli, G.; Dallmeyer, A.; Cabria, I.; Zeller, R.; Dederichs, P. H.; Kern, K.; Carbone, C.; Brune, H. *Science* **2003**, *300*, 1130.
- (46) Smogunov, A.; Dal Corso, A.; Delin, A.; Weht, R.; Tosatti, E. *Nat. Nanotechnol.* **2008**, *3*, 22.
- (47) An, W.; Wu, X.; Yang, J. L.; Zeng, X. C. *J. Phys. Chem. C* **2007**, *111*, 14105.
- (48) Gambardella, P.; Dallmeyer, A.; Maiti, K.; Malagoli, M. C.; Eberhardt, W.; Kern, K.; Carbone, C. *Nature* **2002**, *416*, 301.
- (49) Acharya, C. K.; Turner, C. H. *J. Phys. Chem. C* **2007**, *111*, 14804.

JP9000913